Ceramics International xxx (xxxx) xxx

Contents lists available at ScienceDirect

Ceramics International

journal homepage: www.elsevier.com/locate/ceramint

Mechanical properties of room-temperature injection molded, pressurelessly sintered boron carbide

Erich A. Weaver, Benjamin T. Stegman, Rodney W. Trice, Jeffrey P. Youngblood *

School of Materials Engineering, Purdue University, West Lafayette, IN, 47907, USA

ARTICLE INFO

Keywords:
Carbides
Injection molding
Sintering
Suspensions
Microstructure-final
Electron microscopy
Hardness
Mechanical properties
Armor

ABSTRACT

Boron carbide (B_4C) is of interest in the armor community due to its combination of extreme hardness and low density. However, it is difficult to utilize these properties in many applications due to the challenges associated with forming near-net shapes of B_4C, combined with its low inherent sinterability without the application of external pressure. In this study, highly loaded (51 vol. %) aqueous B_4C suspensions were developed and injection molded at room temperature followed by pressureless sintering up to 2075 °C. Three different sintering aids (Y_2O_3, Al, and Al_2O_3) were used to aid the densification process. B_4C parts were sintered to high density (up to 97.7% relative density) and high hardness values (up to 3200 Vickers). The flexural strength of the samples was limited by grain pullout during polishing of the tensile surface; the strength was correlated to the maximum grain pullout flaw measured at the intersection of the tensile surface and the fracture surface ($R^2 > 0.98$). The robust performance of the B_4C suspensions and their resulting densities and hardness demonstrate the room-temperature injection molding process as a viable alternative for low-cost near-net shaping of B_4C components.

1. Introduction

Boron carbide (B_4C) is known for its high hardness (>3200 Vickers), high melting point (2450 °C), and low density (2.52 g/cm^3) [1]. It is widely used in abrasive applications such as sand-blasting nozzles, grinding and polishing media, water jet cutter nozzles, and wear-resistant coatings. The high hardness of B_4C also makes it an ideal material for lightweight armor applications. Due to the neutron absorption cross-section of boron, B_4C is also used in nuclear reactors [2]. Unfortunately, the beneficial properties of B_4C can only be realized using nearly pore-free, fully dense bodies. However, sintering B_4C is challenging due to densification mechanisms, such as grain boundary and bulk diffusion, becoming effective only at temperatures >2200 °C. Historically, the challenges associated with sintering B_4C have been overcome through the addition of pressure during the sintering process, typically through hot-pressing [1]. The drawback to hot-pressing is that only simple geometric shapes can be produced; any complex features or internal structures will be eliminated by the high uniaxial pressures involved. To produce commercially viable B_4C components with complex geometries, methods other than pressure-assisted sintering must be used.

Injection molding is an appealing method for producing ceramic components due to the ability to produce many near-net shaped parts quickly at low cost [3–5]. Traditional injection molding is accomplished by heating a polymer/ceramic mixture, injecting it into a mold, then removing the heat [3,4]. Ceramics such as SiO_2, SiC, and Al_2O_3 have been injection molded in the past by blending up to 30 vol.% of the desired ceramic powder with a polymer [3]. However, this approach to injection molding requires multiple heating and cooling cycles, along with lengthy polymer burnout cycles prior to sintering. In addition, even when the organic materials are eliminated, the resulting porosity can make sintering difficult. Our prior work has developed an alternative method for injection molding ceramic suspensions that removes or reduces the limitations of traditional injection molding [5–8].

Beginning with highly loaded (>50 vol. %) water-based suspensions that are flowable at room temperature, the rheological properties of the ceramic-polymer suspension is designed to be yield-pseudoplastic. These suspensions will not flow until their yield point is reached, at which point they become shear thinning [9]. This unique behavior allows the suspension to both flow into the mold at room temperature and retain its shape after removal of the stress. Parts made this way are subsequently dried, and de-molded. Less than 5 vol.% polymer binder is added, greatly simplifying the burnout process [7,8,10]. Extensive work has been performed to develop a suspension system for B_4C [10]. The

* Corresponding author.
E-mail address: jpyoungb@purdue.edu (J.P. Youngblood).

https://doi.org/10.1016/j.ceramint.2022.01.015
Received 20 November 2021; Received in revised form 31 December 2021; Accepted 3 January 2022
Available online 19 January 2022

suspensions are electrosterically stabilized using a combination of polyethylenimine (PEI) and hydrochloric acid (HCl) and are robust in that small amounts of sintering aids can be added without causing drastic changes in suspension rheology [10]. However, the challenge of densifying these parts while maintaining their complex features remains.

Even though injection molding offers a route to complex shapes, unfortunately, hotpressing to achieve high density is not a viable method in these cases. Thus, these shapes should be densified with a method such as pressureless sintering to maintain the shape. In many systems, sintering aids are a potential means of densifying a ceramic at lower temperature. Sintering aids have also been widely shown to improve the densification, microstructure, and mechanical properties of B_4C [10–13]. Carbon has been the most widely used sintering aid for B_4C industrially. Lee and Speyer added carbon to pressurelessly sinter B_4C to produce parts of greater than 98% theoretical density [11]. Bougoin and Thevenot added polycarbosilane to pressurelessly sintered B_4C to produce dense composites of B_4C and silicon carbide (SiC) [14]. It has been proposed that carbon benefits densification by reacting with the layer of B_2O_3 on particle surfaces, allowing earlier contact between particles [11,15]. Sintering aids that undergo a reaction during the sintering process to form new phases are of interest as these phases are often liquid at the sintering temperature, and have a beneficial effect on densification.

Commonly during liquid-phase sintering, particles of a distinct second phase are added to the B_4C powder during green body formation. This second phase has a lower melting temperature than the bulk phase and forms a liquid during the heating process. Alternatively, as is commonly the case for B_4C and its sintering aids, a reaction can occur between B_4C and the sintering aid that results in a lower melting point phase forming in-situ during the sintering process. Several systems with potential for liquid-phase-forming reactions with B_4C have been studied, typically either metal oxides or borides. These compounds undergo reactions with B_4C and/or the thin layer of B_2O_3 on particle surfaces to form liquid phases containing a metal, boron, and carbon. Examples include aluminum oxide (Al_2O_3), yttrium oxide (Y_2O_3), titanium oxide (TiO_2), titanium boride (TiB_2) chromium carbide (Cr_3C_2), chromium oxide (Cr_2O_3) and zirconium oxide (ZrO_2) [12,13,16–22].

Several studies in the literature have noted the beneficial effect of using oxide sintering aids for B_4C [12,13,21,22]. Goldstein et al. explored a wide variety of B_4C + metal oxide composites and reported the in-situ formation of metal boride phases that formed through a reaction between the oxides and B_4C [12]. Notably the 8 vol. % Y_2O_3 composition resulted in high density while requiring a relatively small amount of metal oxide. Levin et al. directly studied the effects of both Ti and TiO_2 and found that TiO_2 was more beneficial when compared to Ti when normalized for Ti content [13]. This was attributed to the formation of sub-stoichiometric B_4C leading to increased carbon and boron diffusion. Mashhadi et al. used small additions of aluminum (4 wt. %) to produce parts up to 94% dense and saw a notable increase in flexural strength [23]. Kim et al. hot pressed B_4C with Al_2O_3 additions to nearly full density and reported an increase in hardness and flexural strength [22].

In this work, room-temperature injection molding of highly loaded (51 vol. %) aqueous B_4C suspensions was investigated as a method for producing near-net shape B_4C components. Three sintering aids: Al, Al_2O_3, and Y_2O_3 were identified for use in this study due to their ability to produce B_4C components of high density while only requiring small amounts of additives [12,13,23]. The behavior of these suspensions is characterized, and the microstructure and mechanical properties of the resulting parts is observed and discussed.

2. Experimental approach

2.1. Suspension preparation and characterization

Boron carbide powder (HS Grade, H.C. Stark, Hermsdorf, Germany) was used in this study; these powders had a company specified mean particle size (d_{50}) of 1.1 μm and a specific surface area (SSA) of 17 m^2/g. Y_2O_3 powders (REacton 99.99%, Alfa Aesar, Tewksbury, MA) with a d_{50} of 4.61 μm and a SSA of 3.8 m^2/g, were used as a sintering aid. Aluminum powders (US Research Nanomaterials, Houston, TX) with a d_{50} of 1 μm were also employed in this investigation. Aluminum oxide powders used had a d_{50} of 0.4 μm and an SSA of 8.4 m^2/g (A 16 SG, Almantis, Ludwigshafen, Germany). Table 1 shows a summary of the different compositions investigated in this study. Throughout the work Al_2O_3 content is controlled so that after undergoing a reaction with B_4C during sintering the amount of Al remaining is equal to that found in the metallic Al samples. As an example, 1.87 wt.% Al_2O_3 and 1 wt.% Al samples contain the same amount of Al. The small amount of sintering aids used both reduces the amount of variation in suspension rheology and keeps the theoretical density of final sintered parts at a minimum.

Previous work has found that attrition milling B_4C powders prior to suspension preparation substantially improved suspension rheology by reducing suspension viscosity and yield points [10]. The B_4C powder was attrition milled in ethanol for 2 h at 50 rpm using 3 mm tungsten carbide/cobalt (WC-Co) balls as milling media. Due to the hardness difference between B_4C and WC-Co, the milling media slowly wear down over time and WC is incorporated into the B_4C powder. The exact amount varies between batches and was determined individually for each batch by weighing the milling media before and after attrition milling. The amount of WC-Co incorporated varied from 3 to 8 wt. %; individual batches were mixed to normalize the amount of WC-Co in each to have a final composition of 5 wt. % WC-Co.

Our previous study on B_4C suspensions found that PEI with a molecular weight of 25,000 g/mol acts as an excellent electrostatic dispersant for B_4C powders [10]. The ideal amount of dispersant was found to be 1.83 mg/m^2 (relative to the surface area of the ceramic powder). Hydrochloric acid (HCl) was used to modify the pH of the suspensions for increased dispersion. The amounts of PEI and HCl used in this study were both 3.57 vol. %.

Suspensions were prepared by mixing the dispersant and HCl with reverse osmosis (RO) water in a dual-centrifugal speed mixer (DAC 400, Flacktek Inc., Landrum, SC). B_4C and the sintering aid were then added in small (15–20 g) increments. Mixing increments were performed for 1 min at 800 rpm followed by 1 min at 1200 rpm, with the total mixing time taking less than 30 min. After mixing, five 12.5 mm WC-Co milling media were added, and the suspension was ball milled for approximately 24 h.

Table 1
Composition of B_4C suspensions used in injection molding experiments.

Sample Name	Sintering Aid	Sintering Aid Amount (wt. %)	WC-Co Content (wt. %)	Dispersant Content (vol. %)	HCl Content (vol. %)
B_4C	N/A	N/A	5	3.57	3.57
5 wt. % Y_2O_3	Y_2O_3	5	5	3.57	3.57
10 wt. % Y_2O_3	Y_2O_3	10	5	3.57	3.57
15 wt. % Y_2O_3	Y_2O_3	15	5	3.57	3.57
1 wt. % Al	Al	1	5	3.57	3.57
2 wt. % Al	Al	2	5	3.57	3.57
3 wt. % Al	Al	3	5	3.57	3.57
1.87 wt. % Al_2O_3	Al_2O_3	1.87	5	3.57	3.57
3.71 wt. % Al_2O_3	Al_2O_3	3.71	5	3.57	3.57
5.52 wt. % Al_2O_3	Al_2O_3	5.52	5	3.57	3.57

The rheological properties of the suspensions were measured using a Malvern Bohlin Gemini HR Nano rheometer (Malvern Instruments Ltd., Worcestshire, UK) with a CP 4°/40 cone and plate measuring system and a 150 μm gap size. Approximately 1 mL of suspension was used for each test with a water trap to prevent the suspension from drying out prematurely during testing. A pre-shear of 1 s^{-1} was applied before each test to ensure each sample had an identical shear history. A logarithmic table of shears from 0.005 to 500 s^{-1} was applied to measure the viscosity and shear stress of each sample. During room-temperature injection molding the shear rate is estimated to be 10 s^{-1} (with a syringe diameter of 2.1 mm and an MTS crosshead speed of 25 mm/min applied to the syringe).

2.2. Room-temperature injection molding

Fig. 1 provides an overview of the room-temperature injection molding process. All injection molds were made from a polymer resin; this was possible because the suspension was designed to flow at room temperature. A mold, shown in Fig. 2, was designed to produce a rectangular billet green body with dimensions of 7 × 25 × 75 mm. The

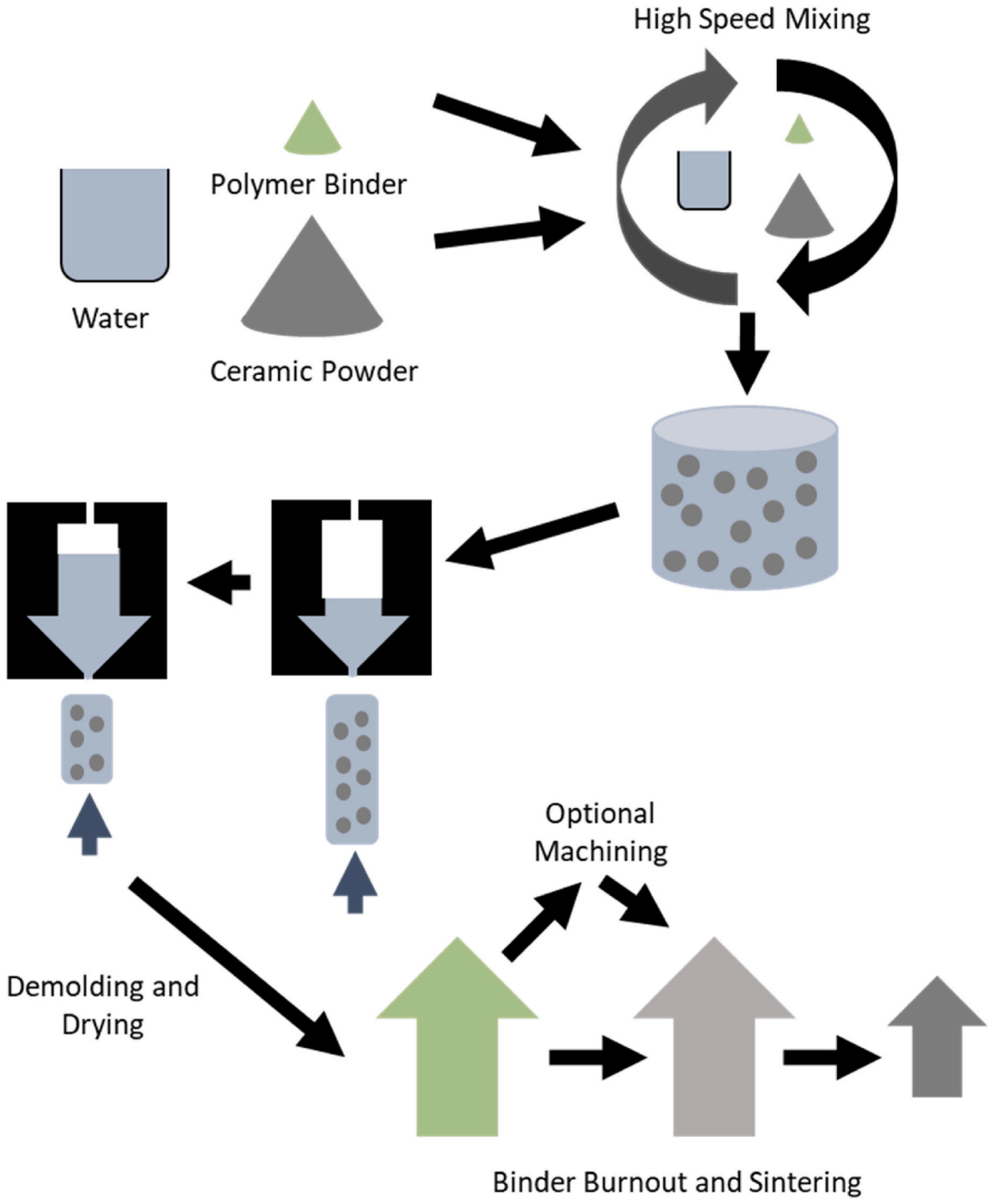

Fig. 1. Summary of the injection molding process. Suspensions are prepared by mixing water, ceramic, powder, and a polymer dispersant. They were then injection molded and allowed to dry before undergoing binder burnout and sintering.

Fig. 2. A) Three-piece mold used for injection molding and B) assembled view.

middle section of the mold was created using a Form 2 (Formlabs, Somerville, MA) stereolithography (SLA) 3-D printer. The design included three 2 mm diameter vents to allow air and excess material to escape during injection molding and an injection port sized to fit a Luer-Lock syringe tip. The top and bottom sections of the mold were cut from an acrylic sheet and had a layer of PTFE tape adhered to the inner surface. Wetted ashless filter paper (Grade 40, Whatman, UK) was applied to the top and bottom sections of the mold to aid the drying process and prevent cracking.

B_4C suspensions were loaded into a 50 mL syringe with a Luer-Lock tip. In an attempt to remove any potential air bubbles introduced during syringe filling, the filled syringe was attached to an empty syringe using a small hose. Air bubbles were removed by passing the suspension between the two syringes. The filled syringe tip was then inserted into the injection port on the mold, and the entire assembly placed in an MTS load frame (MTS Insight 100, MTS Systems Corporation, Eden Prairie, MN). The MTS crosshead speed was set to 25 mm/min, resulting in a total injection time of approximately 1 min. Once injected, the top acrylic plate of the mold was removed to speed the drying process and samples were allowed to air-dry for 45 min prior to carefully removing the top filter paper. Each sample was then placed in a desiccator maintained at 30% relative humidity by a sulfuric acid and water solution. After 24 h, each sample was completely demolded and placed back in the desiccator to finish drying (approximately 96 h).

2.3. Binder burnout and sintering

Once demolded and dried, samples underwent binder burnout to remove all organic compounds. Samples were placed in a tube furnace with flowing Argon (Ar) at a heating rate of 1 °C/min to 500 °C where they were held for 25 h. A previous study showed thermogravimetric analysis (TGA) results with a complete pyrolysis of PEI in a flowing Ar atmosphere below 500 °C [10]. Samples were then placed in a graphite crucible and sintered in a Centorr Testor Furnace (Centorr Vacuum Industries, Nashua, NH) in a flowing Ar atmosphere purified in a 2G-100-SS Centorr Gettering Furnace to less than 10^{-7} ppm O_2. Heating at a rate of 25 °C/min to 2075 °C, followed by a 4 h hold, was used to densify the parts.

2.4. Characterization

After sintering, the triangular runner section of each billet was cut using a diamond-tipped saw blade. These sections were then mounted and polished, finishing with a 1 μm diamond suspension. Hardness testing was performed on a Wilson Hardness Tukon 1202 using a Vickers head with a test force of 9.81 N and a hold time of 10 s in accordance with ASTM C1327-15. A minimum of ten indents were optically measured for each sample. X-ray diffraction was performed for each composition using a Bruker D-8 Focus (Bruker, Madison, WI). Scanning electron microscopy of polished samples (coated with a layer of Au/Pt) was performed on a FEI Quanta 650 SEM at 15 kV (Thermofisher Scientific, Waltham, MA).

Size B (3 × 4 × 45 mm) flexure bars were machined (Bomas Machine Specialties, Inc., Somerville, MA) from each sintered billet in accordance with ASTM C1161-18. Before testing, the relative density of each sample was measured. The apparent density of each sample was determined using the Archimedes' method. The theoretical density for each composition was calculated using the rule of mixtures with densities of 2.52 g/cm^3, 14.6 g/cm^3, 5.01 g/cm^3, 2.70 g/cm^3, and 3.95 g/cm^3 used for B_4C, WC-Co, Y_2O_3, Al, and Al_2O_3 respectively. Flexure testing was performed using an MTS machine and a 4-point semi-articulated fixture with the crosshead speed set to 0.5 mm/min. For each composition, a minimum of seven tests were performed, and the Weibull modulus and characteristic strength were calculated in accordance with ASTM C1239-13.

After testing, the tensile edge of the fracture surface of each flexure bar was optically imaged (Olympus GX41, Olympus Corporation, Lombard, IL). Using ImageJ software, each flaw along the fracture surface was measured, and an average flaw size and maximum flaw size was determined for each sample. Select bend bar fragments were mounted, polished, and electrochemically etched in a 1% potassium hydroxide (KOH) solution (Fisher Chemical, Waltham, MA) with a DC current of 20 V for 3–5 s. The etched surfaces were optically imaged, and an average grain size was determined using the line-intercept method.

3. Results and discussion

3.1. Characterization of ceramic suspensions

The rheological behavior of suspensions used in this study is presented in Fig. 3. A more comprehensive exploration of the rheological behavior of suspensions containing only B_4C powers (no sintering aids) was been published previously [10]. Colloidal processing of multiple component systems can change the rheology of suspensions, with minimum data in the literature available for the highly loaded B_4C suspensions like those studied here. For this study, it is sufficient to note that sintering aid particles (even in the relatively small amounts used) did have some influence on suspension rheology. Fig. 3A shows the viscosity versus applied shear rate of a characteristic suspension for each sintering aid as well as a B_4C suspension with no sintering aid, while the shear stress as a function of applied shear rate is shown in Fig. 3B. Both the Al and Al_2O_3 suspensions had similar yield points than the suspensions with no sintering aid, while the Y_2O_3 suspension had a slightly higher yield point. All suspensions demonstrated yield-pseudoplastic behavior ideal for injection molding. The yield point in each suspension can be attributed to flocculation of the ceramic particles. This yield

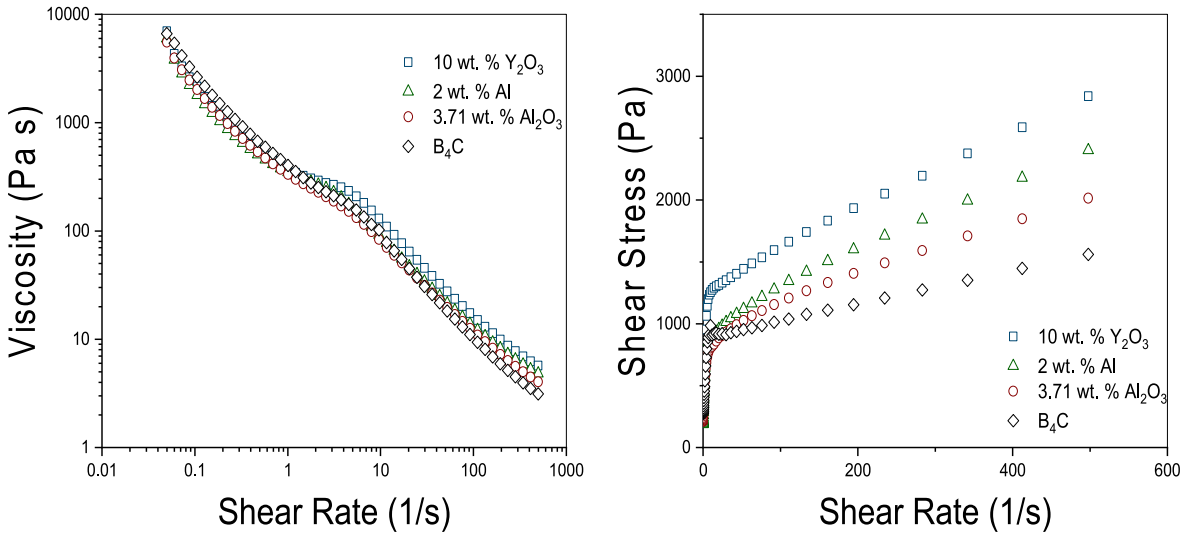

Fig. 3. A) Viscosity of three of the suspensions used in this study as a function of applied shear rate at room temperature. The estimated shear rate during injection molding is 10 s^{-1}. B) The shear stress versus shear rate for the same suspensions.

point can also be observed in the viscosity versus applied shear rate graph as a transition in the slope of the graphs at an approximate shear rate of 3 s^{-1}. At higher shear rates (e.g. those used in the injection molding process) the flocs of ceramic particles are broken up and flow becomes much easier. Explaining the exact cause of the difference in yield point between suspensions is difficult as a wide variety of factors such as particle size, size ratios, and surface charges can affect floc size and strength [24]. However, all suspensions were still flowable at room temperature and behaved similarly during injection molding.

3.2. Injected molded sample characterization

A summary of the mechanical properties of each composition used in this study is presented in Table 2, with the average relative density of each composition plotted in Fig. 4. All samples were successfully injection molded and underwent binder burnout without cracking or other defects. The average relative density of boron carbide with no sintering aid was 92.6%, higher than is often reported in literature [12,13,23]. This can be attributed to the presence of WC-Co contamination from attrition milling. WC in amounts up to 10 wt. % has been previously shown to react with boron atoms in B_4C to form W_2B_5 [25,26] and improve density [26]. The addition of Y_2O_3, Al, or Al_2O_3 statistically improved density even further, with two-tailed t-tests resulting in $p \leq 0.002$ for all compositions. Additions of 10 wt. % Y_2O_3 was the most effective sintering aid overall, with an average relative density of 97.7%. The 1 wt. % Al and 1.87 wt. % Al_2O_3 compositions also achieved high relative densities of 96.9% and 95.7%, respectively.

It had been previously proposed by Levin et al. [13] that metal oxides acted as more efficient sintering aids than their base metals due to the oxygen atoms creating carbon vacancies to aid lattice diffusion during sintering. In this study, additions of Al_2O_3 were normalized to match Al content. For normalized 1 and 2 wt. % Al, the relative densities were statistically similar ($p = 0.57$ and $p = 0.07$ respectively). For normalized 3 wt. % Al, the oxide addition was statistically less dense than the metal base ($p = 0.01$). This difference can likely be explained by the fact that in the Ti/TiO_2 study, greater amounts of sintering aid (up to 25 wt. %) were used, which would cause a much larger amounts of boron depletion in the B_4C microstructure than the small amounts of sintering aid (<5 wt. %) used in the present study. In fact, when small amounts of Ti/TiO_2 were used, the resulting density differences were much smaller, similar

Table 2
Mechanical properties of sintered B_4C bars of each composition used in this study.

Sample Name	Maximum Sintered Relative Density (%)	Average Sintered Relative Density (%)	Vickers Hardness (HV)	Average Four-Point Flexural Strength (MPa)	Characteristic Strength (MPa)	90% Confidence Bounds	Weibull Modulus	90% Confidence Bounds	Average Grain Size (μm)
B_4C	92.6	90.0 ± 0.5	2470 ± 47	295.3 ± 15.2	322	292–356	8.6	3.9–12.1	2.9 ± 0.1
5 wt. % Y_2O_3	94.8	92.7 ± 0.5	2994 ± 41	176.6 ± 5.7	184	170–200	9.5	4.7–13.2	32.4 ± 1.1
10 wt. % Y_2O_3	97.7	95.5 ± 0.5	3208 ± 53	212.4 ± 3.6	218	209–227	18.4	9.7–25.2	41.3 ± 0.7
15 wt. % Y_2O_3	95.6	94.8 ± 0.2	3148 ± 66	150.0 ± 2.3	153	148–158	20.4	10.8–28.0	58.7 ± 1.3
1 wt. % Al	96.9	93.5 ± 0.4	2911 ± 38	274.3 ± 7.0	285	268–303	11.5	6.1–15.8	10.8 ± 1.5
2 wt. % Al	95.1	93.9 ± 0.4	3000 ± 39	261.3 ± 13.0	290	269–313	11.3	5.2–15.9	13.2 ± 1.3
3 wt. % Al	95.1	94.2 ± 0.2	3076 ± 21	265.5 ± 8.9	276	251–306	9.9	4.1–14.2	10.6 ± 1.6
1.87 wt. % Al_2O_3	95.7	92.9 ± 0.8	2954 ± 32	271.3 ± 19.0	304	264–352	5.3	2.6–7.4	9.5 ± 2.3
3.71 wt. % Al_2O_3	95.2	94.7 ± 0.1	3004 ± 33	254.9 ± 10.2	267	241–298	7.9	3.7–11.3	10.4 ± 3.8
5.52 wt. % Al_2O_3	94.1	93.4 ± 0.2	3116 ± 28	265.1 ± 10.0	279	256–306	7.9	4.2–10.8	8.1 ± 1.6

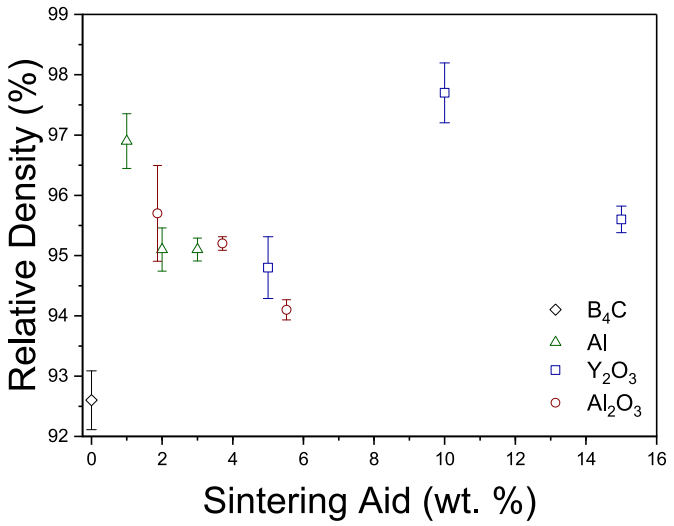

Fig. 4. Maximum relative density of each of the compositions used in this study. The amounts of Al_2O_3 were chosen to correspond to the amounts of Al after a reduction during sintering.

to those seen in the present study [13].

3.3. Effect of sintering aid choice on microstructure

A representative microstructure for each sintering aid is shown in Fig. 5. All three sintering aids react with B_4C at during sintering, forming a liquid, and ultimately Metal-B-C phases upon cooling [12,21,23]. XRD (see Figs. 6 and 7) confirmed the presence of these phases. Specifically, the Y_2O_3 specimens formed a composition of YB_4, YB_6, YB_2C, and YB_2C_2 which matched the observations made by Goldstein et al. [12]. The Al and Al_2O_3 specimens both formed AlB_2 and Al_3BC, which matched the observations made by Mashhadi et al. [23]. All secondary phases are found as multigrain aggregates between B_4C grains in the as-sintered

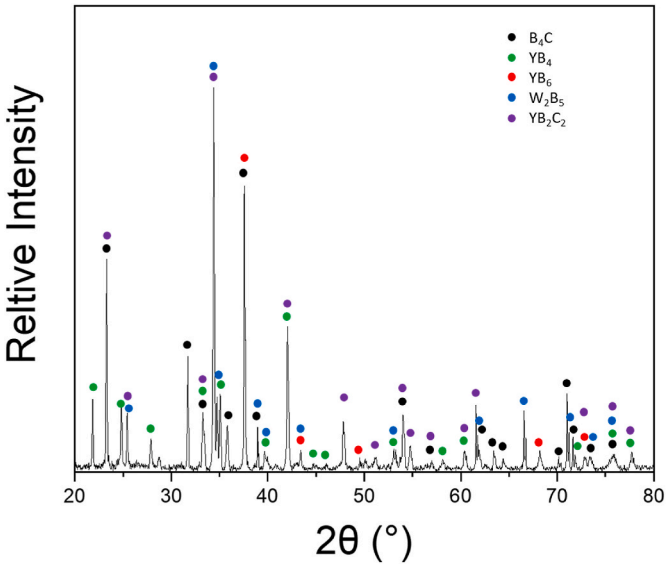

Fig. 6. XRD patterns showing phase compositions of specimens sintered using Y_2O_3 as a sintering aid.

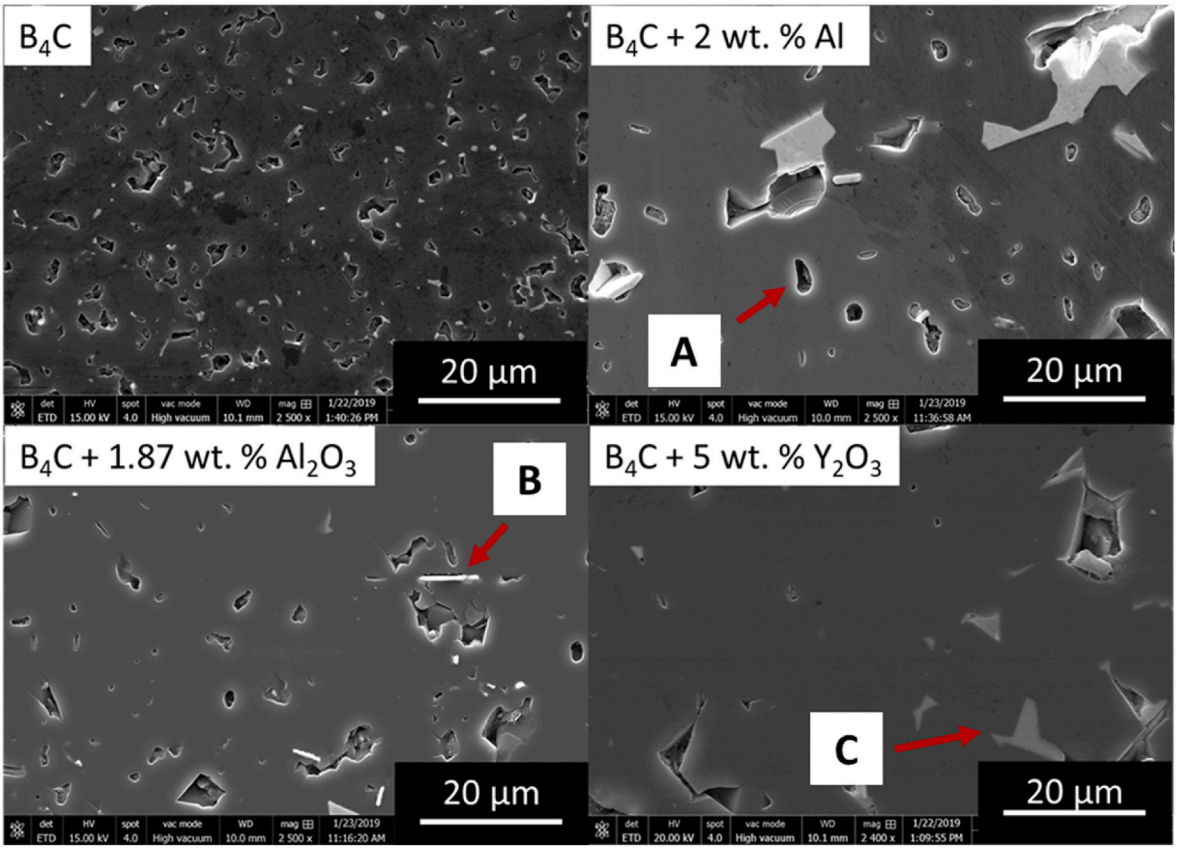

Fig. 5. Representative microstructures for each of the sintering aids used in this study. Sintering aid phases form in the areas between B_4C grains. The WC-Co contamination from attrition milling forms W_2B_5 platelets regardless of which sintering aid is used. *(A)* Porosity due to incomplete sintering. *(B)* W_2B_5 platelet. *(C)* Secondary sintering aid phase.

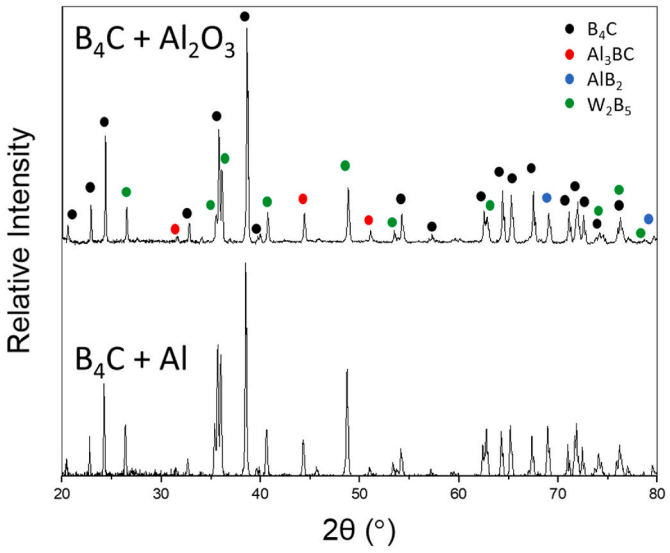

Fig. 7. XRD pattern showing phase compositions of specimens sintered using Al and Al_2O_3 sintering aids.

microstructures.

The WC-Co also undergoes a reaction during sintering to form W_2B_5 platelets [25,26]. These platelets have a high aspect ratio and, interestingly, are often found at the boundary between B_4C grains and other secondary phases [26]. Tungsten is soluble in both aluminum and yttrium at high temperatures [27], suggesting that tungsten dissolves into the liquids formed during sintering and then precipitates to form W_2B_5 platelets. This effect is most pronounced in the Y_2O_3 samples, likely because those samples contain the largest amount of sintering aid, and therefore the highest volume fraction of liquid phases during the sintering process (see supporting Figure A1). The high aspect ratios of many of these particles suggest an interface-controlled growth mechanism, which further supports the proposed mechanism of solution-precipitation (as diffusion through solid B_4C would be significantly slower). Phases containing Co were not identifiable in any of the XRD plots, suggesting Co is held in solid solution in one of the other phases or Co phases are present in amounts too small to be detected.

3.4. Effect of sintering aids on mechanical behavior

A summary of the mechanical properties of each composition used in this study is presented in Table 2. The Vickers hardness as a function of the sintering aids is shown in Fig. 8. The samples with no sintering aid had hardness values significantly below that of commercially available B_4C; this can be attributed to their lower density. There was no statistical difference between the Al and Al_2O_3 sintering aids with respect to hardness values. This is as expected due to Al and Al_2O_3 forming the same Metal-B-C phases during the sintering process (Fig. 6). The best performing compositions containing Al demonstrated hardness results similar to previous work using Al as a sintering aid (the authors were unable to find reported literature values for pressurelessly sintered B_4C with added Al_2O_3) [23]. Using 10 wt. % Y_2O_3 demonstrated the highest overall hardness, with an average value of 3208 Vickers. This can be explained by the reduction of Y_2O_3 during the sintering process. Free carbon has been shown to decrease the hardness of B_4C [1], and the B_4C powder used in this study contained small amounts of free carbon (as do many commercially manufactured powders. During the sintering process this carbon is off-gassed as CO as Y_2O_3 reduces. To the best of our knowledge, this is the highest hardness value for a B_4C/Y_2O_3 composite reported in the literature.

The average four-point flexural strength of each composition is shown in Fig. 9. All flexure bars failed in the middle of the sample, within the inner span of four-point bend fixture (See supporting Figure A2). It was expected that as density increased with the addition of sintering aids, flexural strength would also increase. It has been widely reported in literature that sintering aids increase flexural strength, with the maximum flexural strength usually corresponding to the highest density [12,13,18,23]. Despite its lower average density, the flexural strength of B_4C with no sintering aids had the highest average value among all samples. The Al and Al_2O_3 had similar flexure values when normalized for Al content, with no statistical significance between them (all $p < 0.001$). Y_2O_3 samples had the lowest flexural strength overall, with 10 wt. % Y_2O_3 having an average flexural strength of 212.4 MPa Y_2O_3 samples had the most consistent results, with the smallest standard deviation across all samples tested. Due to the dependence of the flexural strength of B_4C on the amount and type of sintering aid used, as well as different sintering parameters, it can be difficult to compare to values in the literature. Mashhadi et al. reported a flexural strength of 270 MPa for B_4C samples with 4 wt. % Al, sintered at 2150 °C to densities of approximately 95% [23]. Goldstein et al. demonstrated flexural strengths ranging from 160 to 200 MPa for 8 vol. % Y_2O_3 (approximately 15 wt. %) sintered at 2180 °C to 97.5% density.

The Weibull plots of flexural strength of the composition with the highest Weibull modulus for each sintering aid are shown in Fig. 10. The complete Weibull parameters for each composition, along with their

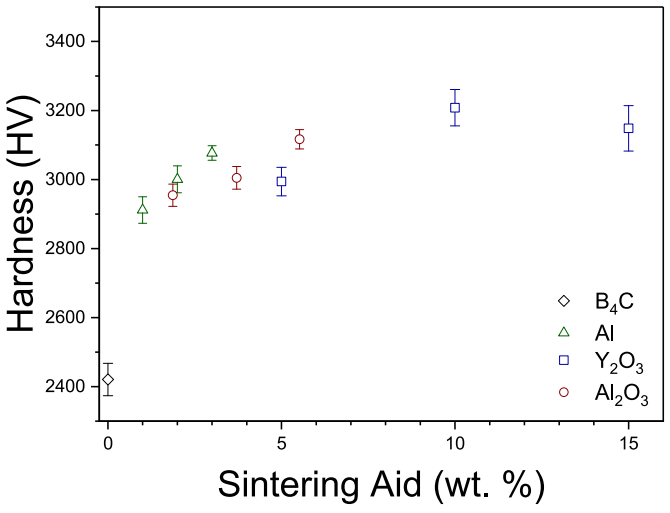

Fig. 8. Average Vickers hardness of each of the compositions used in this study.

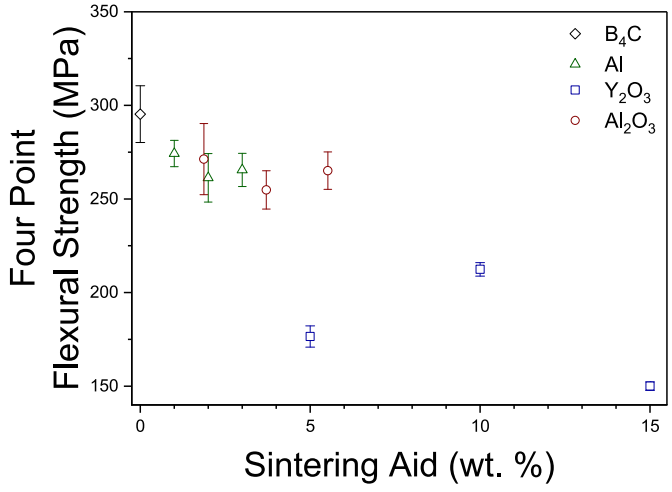

Fig. 9. Average four-point flexural strength for each composition used in this study.

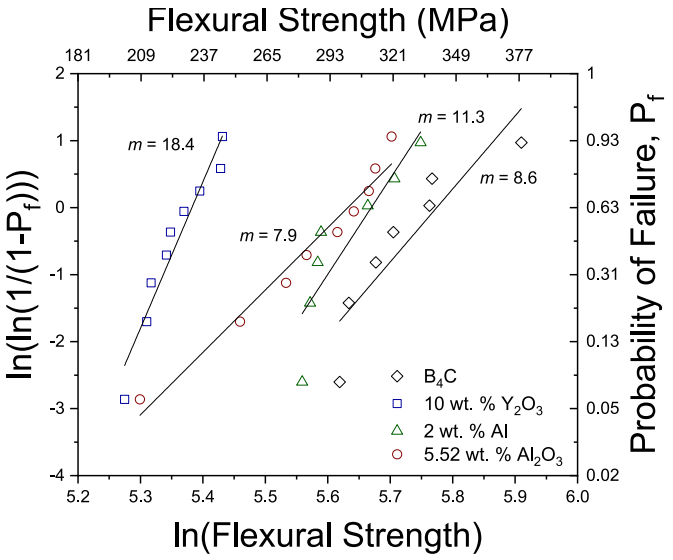

Fig. 10. Weibull plots of the flexural strength of B_4C samples made using each type of sintering aid.

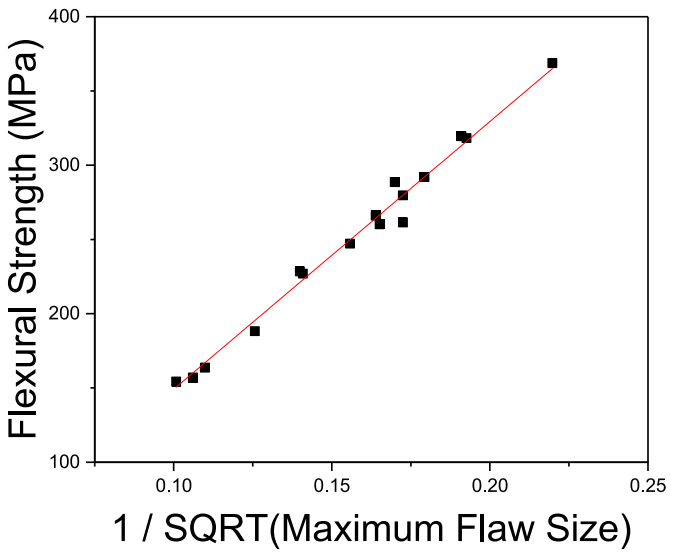

Fig. 11. Plot of flexural strength versus the maximum flaw size measured on the intersection of the fracture face and tensile surface. Specimens were randomly selected from each composition.

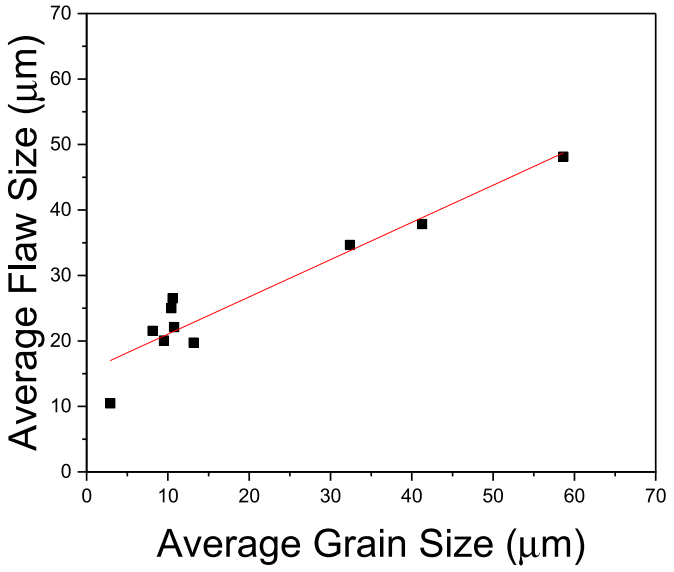

Fig. 12. Plot of average grain size of each composition versus the average flaw size on the intersection of the fracture face and the tensile surface. Larger grain size lead to larger flaws on the tensile surface due to grain pullout.

90% confidence bounds, can be found in Table 2. Due to the small number of samples tested in this study, there is a high uncertainty associated with the parameter estimates that can be seen in the confidence bounds. The Y_2O_3 samples had the highest Weibull modulus, indicating the lowest scatter in their flexural strengths. The 1.87 wt. % Al_2O_3 sample had the lowest Weibull modulus of 5.3, indicating it had the largest spread in its flexural strength values. The 90% confidence bounds for the Weibull moduli are large, so it is difficult to determine if the Weibull modulus for each composition are significantly different.

Due to the lack of obvious macro pores in any of the sample, the primary defect for Weibull analysis was initially assumed to be small pores from incomplete sintering. However, optical examination of the tensile surface of the flexure specimens revealed significant grain pull-out present across all samples (see supporting Figure A3). The stress profile of a four-point flexure test places the maximum tensile stress on a wide region of the tensile surface of the sample. It can be assumed that the largest flaw (i.e. grain pulled out) on the tensile surface is the primary cause of failure and should be present along the intersection of the tensile surface and the fracture surface. This intersection was imaged for randomly selected samples across all compositions, and the maximum flaw size on each sample was measured using ImageJ software. A plot of flexure strength vs. the inverse square root of the maximum measured flaw size is shown in Fig. 11. There is a strong positive correlation between the maximum flaw size and the flexural strength, with an R^2 value > 0.98. The presence of "artificially" created flaws indicates that the true flexural strength of these compositions may be higher than the values reported in this study.

If the maximum flaw size on the tensile surface is caused by grain pullout, it follows that flexure strength should be similarly correlated to grain size. While it is impossible to determine the largest grain present on the tensile surface of any given sample, the average grain size can be readily determined using the line intercept method. The average grain size vs. average flaw size for each composition is plotted in Fig. 12. There is a large positive correlation between average grain size and average flaw size with an R^2 value > 0.9. The Y_2O_3 composition, which had the largest average grain sizes, also had the largest average flaw sizes while the undoped B_4C samples had both the smallest average grain size and the smallest average flaw size. All the sintering aids used in this study significantly increased grain size (with the smallest increase, 1.87 wt. % Al_2O_3, effectively tripling the grain size), leading to larger flaws from grain pullout which explains the drop in flexural strength. Modifying the sintering parameters used in this study to reduce grain growth while maintaining high relative densities should help increase the flexural strength of samples made with these sintering aids, particularly Y_2O_3.

4. Conclusions

Room-temperature injection molding was used to prepare green bodies of highly loaded (51 vol. % solids), aqueous B_4C suspensions. Samples underwent binder burnout and pressureless sintering at 2075 °C without any cracking or warpage defects. Undoped B_4C and three sintering aids (Y_2O_3, Al, and Al_2O_3) were tested, with all three sintering aids leading to high relative densities (>95%). The most promising sintering aid identified was 10 wt. % Y_2O_3 due to having the highest relative density (97.7%) and Vickers hardness values (3208 GPa). The composition also had a high Weibull modulus of 18.4, the second highest of all samples tested. The flexural strength of the samples was negatively affected by grain pullout during polishing of the tensile

surfaces. This grain pullout worsened as grain size increased, indicating that modifying sintering parameters to control grain growth could mitigate these issues in future work. Room-temperature injection molding, in conjunction with pressureless sintering aids such as Y_2O_3, could expand the use of B_4C due to its ability to produce near net shapes of high density and favorable mechanical properties.

Declaration of competing interest

The authors declare that they have no known competing financial interests or personal relationships that could have appeared to influence the work reported in this paper.

Acknowledgements

This work was supported by the Office of Naval Research (Award Number N000141712155), the Department of State (Contract No. SAQMMA14D0135), and the National Defense Science and Engineering Graduate Fellowship Program.

Appendix A. Supplementary data

Supplementary data to this article can be found online at https://doi.org/10.1016/j.ceramint.2022.01.015.

References

[1] F. Thévenot, Boron carbide-A comprehensive review, J. Eur. Ceram. Soc. 6 (1990) 205–225.
[2] K. Gillet, G. Roma, J.P. Crocombette, D. Gosset, The influence of irradiation induced vacancies on the mobility of helium in boron carbide, J. Nucl. Mater. 512 (2018) 288–296.
[3] M.J. Edirisinghe, J.R.G. Evans, Review: fabrication of engineering ceramics by injection moulding. I. Materials selection, Int. J. High Technol. Ceram. 2 (1986) 1–31.
[4] M.J. Edirisinghe, J.R.G. Evans, Review: fabrication of engineering ceramics by injection moulding. II. Techniques, Int. J. High Technol. Ceram. 2 (1986) 249–278.
[5] V.L. Wiesner, Fabricating Complex-Shaped Components by Room-Temperature Injection Molding of Aqueous Ceramic Suspension Gels, Purdue University, 2013. Doctoral dissertation.
[6] V.L. Wiesner, J.P. Youngblood, R.W. Trice, Room-temperature injection molding of aqueous alumina-polyvinylpyrrolidone suspensions, J. Eur. Ceram. Soc. 34 (2014) 453–463.
[7] V.L. Wiesner, L.M. Rueschhoff, A.I. Diaz-Cano, RW Trice, JP Youngblood "Producing dense zirconium diboride components by room-temperature injection molding of aqueous ceramic suspensions", Ceram. Int. 42 (2016) 2750–2760.
[8] L.M. Rueschhoff, R.W. Trice, J.P. Youngblood, Near-net shaping of silicon nitride via aqueous room-temperature injection molding and pressureless sintering, Ceram. Int. 43 (2017) 10791–10798.
[9] D.R. Dinger, Rheology for Ceramists, Dinger Ceramic Consulting Service, 2002.
[10] A. Diaz-Cano, Boron Carbide: Stabilization of Highly-Loaded Aqueous Suspensions, Pressureless Sintering, and Room Temperature Injection Molding, 2017. Doctoral dissertation.
[11] H. Lee, R.F. Speyer, Pressureless Sintering of Boron Carbide, vol. 73, 2010, pp. 1468–1473.
[12] A. Goldstein, Y. Yeshurun, A. Goldenberg, B4C/metal boride composites derived from B4C/metal oxide mixtures, J. Eur. Ceram. Soc. 27 (2007) 695–700.
[13] L. Levin, N. Frage, M.P. Dariel, The effect of Ti and TiO 2 additions on the pressureless sintering of B 4 C, Metall. Mater. Trans. 30A (1999) 3201–3210.
[14] M. Bougoin, F. Thevenot, Pressureless sintering of boron carbide with an addition of polycarbosilane, J. Mater. Sci. 22 (1987) 109–114.
[15] S.L. Dole, S. Prochazka, R.H. Doremus, Microstructural coarsening during sintering of boron carbide, J. Am. Ceram. Soc. 72 (1989) 958–966.
[16] P. Ponnusamy, B. Feng, H.P. Martin, P. Groen, Effect of TiB2 nano-inclusions on the thermoelectric properties of boron rich boron carbide, Mater. Today Proc. 5 (2018) 10306–10315.
[17] J. Wu, et al., Effect of titanium diboride on the homogeneity of boron carbide ceramic by flash spark plasma sintering, Ceram. Int. 44 (2018) 15323–15330.
[18] X. Li, et al., Pressureless sintering of boron carbide with Cr3C2 as sintering additive, J. Eur. Ceram. Soc. 34 (2014) 1073–1081.
[19] E. Marek, E. Dudnik, G. Makrenko, E. Remenyuk, Some physical properties of boron carbide with vanadium and chromium additions, Sov. Powder Metall. Met. Ceram. 14 (1975) 130–131.
[20] S. Yamada, Sintering Behavior of B 4 C – CrB 2 Ceramics, vol. 29, 2002, pp. 1445–1447.
[21] C.H. Lee, C.H. Kim, Pressureless sintering and related reaction phenomena of Al2O3-doped B4C, J. Mater. Sci. 27 (1992) 6335–6340.
[22] H. Kim, Y. Koh, H. Kim, Densification and mechanical properties of B4C with Al2O3 as a sintering aid, J. Am. Ceram. Soc. 83 (2004).
[23] M. Mashhadi, E. Taheri-Nassaj, V.M. Sglavo, Pressureless sintering of boron carbide, Ceram. Int. 36 (2010) 151–159.
[24] Derek R. Harding, Heterocoagulation in mixed dispersions—effect of particle size, size ratio, relative concentration, and surface potential of colloidal components, J. Colloid Interface Sci. 40 (1972).
[25] G. Wen, et al., Reaction-formed W2B5/C composites with high performance, Carbon 44 (2006) 1005–1012.
[26] J. Yin, et al., J. Euro. Ceram. Soc vol. 33 (2013) 1647–1654.
[27] E. Lassner, W.D. Schubert, Tungsten Properties, Chemistry, Technology of the Element, Alloys, and Chemical Compounds, Springer Science and Business Media, 1999.